Intermetallic compounds M_2Pt (M = Al, Ga, In, Sn) in the oxygen evolution reaction

Ana María Barrios Jiménez, Alim Ormeci, Ulrich Burkhardt, Simone G. Altendorf, Felix Kaiser, Igor Veremchuk, Gudrun Auffermann, Yuri Grin, Iryna Antonyshyn*

Figures and Tables:

Figure S1. Light optical micrographs and EDXS results for the M_2Pt (M = Al, Ga, In, Sn) samples.

Figure S2. Figure S2. BSE images (material contrast, 27 kV) of the M_2Pt specimens, where M is Al (*a*), Ga (*b*), In (*c*) or Sn (*d*), supported by the elemental mapping for Al_2Pt, Ga_2Pt and In_2Pt, revealing the homogeneity of these samples.

Figure S3. Chemical bonding in Sn_2Pt (*top*) and In_2Pt (*bottom*). Position of the (2a)Pt-Sn and (3a)Pt-In bonds are shown with the ELI-D distributions (*left upper corner*) and isosurfaces (*left bottom corner of each panel*). Bonding basins of these bonds (*yellow*) are shown in overlap with the QTAIM atomic shapes of Pt and Sn for Sn_2Pt (*top*), and Pt and two In for In_2Pt (*bottom*).

Figure S4. Every 5th CV cycle (0.1 M $HClO_4$; 0.05–1.0 V_{RHE}; 50 mV s^{-1}) for the M_2Pt (M = Al, Ga, In, Sn) compounds. The fifth cycle is presented with *dashed* line and following cycles are presented with the *solid* lines of increasing intensity of corresponding color. Insets: 49th and 50th CV cycles for M_2Pt.

Figure S5. Normalized XPS spectra of Pt 4*f* core levels for the M_2Pt compounds before (*dashed lines*) and after CV (*solid lines*). The vertical solid lines represent the position of Pt 4*f* core levels in elemental Pt.

Figure S6. Chronopotentiometry, measured at 10 mA cm^{-2} during 2 h, for the M_2Pt compounds.

Figure S7. XPS spectra of M core levels in M_2Pt compounds before (*dashed lines*) and after the standard OER experiment (*solid lines*). The vertical solid lines represent the binding energies for M_2Pt, M_xO_y oxides and $M(OH)_x$ hydroxides.

Figure S8. Calculated total and orbital projected DOS for the M_2Pt compounds and *fcc* Pt at the fully-relativistic level.

Figure S9. Surface energies of the different Al_2Pt surfaces versus the chemical potential of Al.

Table S1. OER performance of bulk OER electrocatalysts in acidic media: overpotential at 10 mA cm^{-2} (otherwise indicated with the subscript of η) as activity marker, and time of the chronopotentiometry (CP) or chronoamperometry (CA) operation at j = 10 mA cm^{-2} (otherwise indicated) as stability marker.

Table S2. The XPS binding energies of Pt $4f_{7/2}$ core levels (BE_{4f}) and their shifts ($\delta(BE_{4f})$, with respect to elemental Pt) in the intermetallic M_2Pt compounds.

Table S3. Calculated (for homogeneous M_2Pt) and experimentally obtained (with EDXS, for samples after the standard OER experiment) intensities of the M line spectra (in cps/eV) normalized to the Pt $M\alpha$ (using different acceleration voltages).

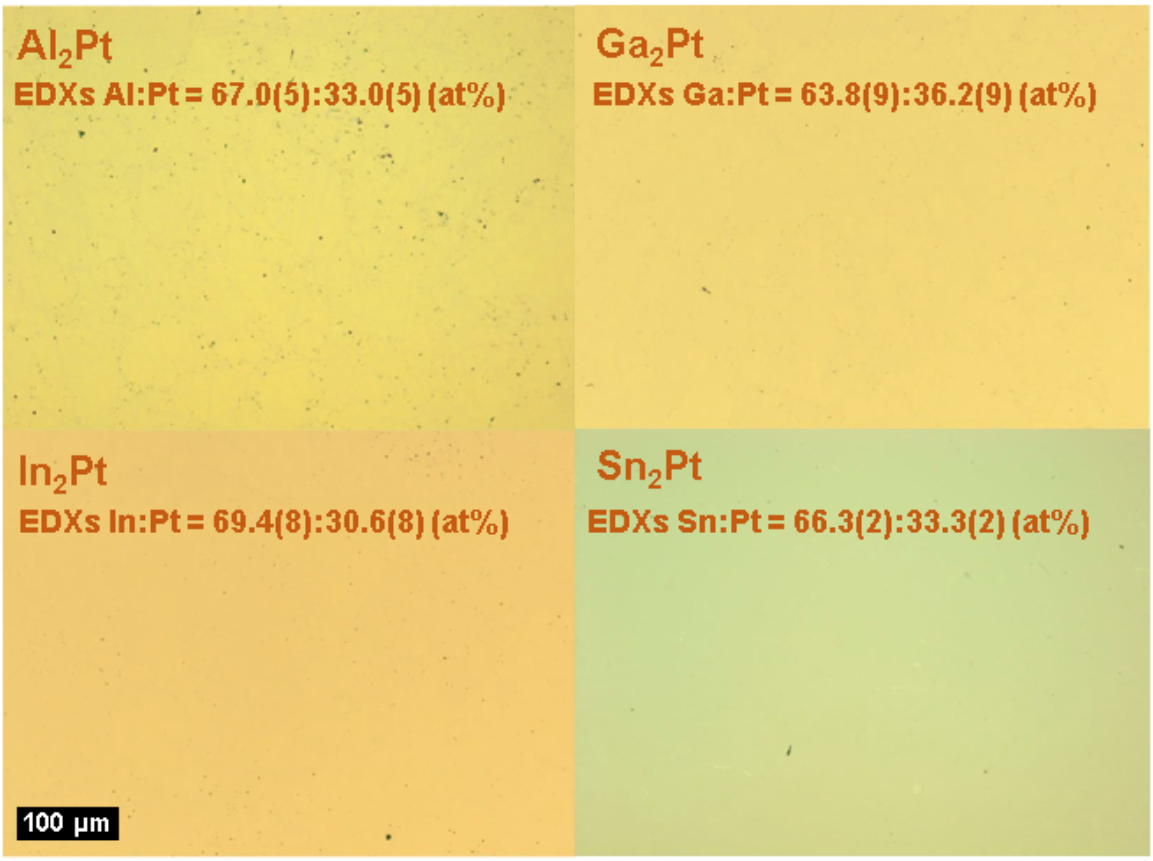

Figure S1. Light optical micrographs and EDXS results for the M_2Pt (M = Al, Ga, In, Sn) samples.

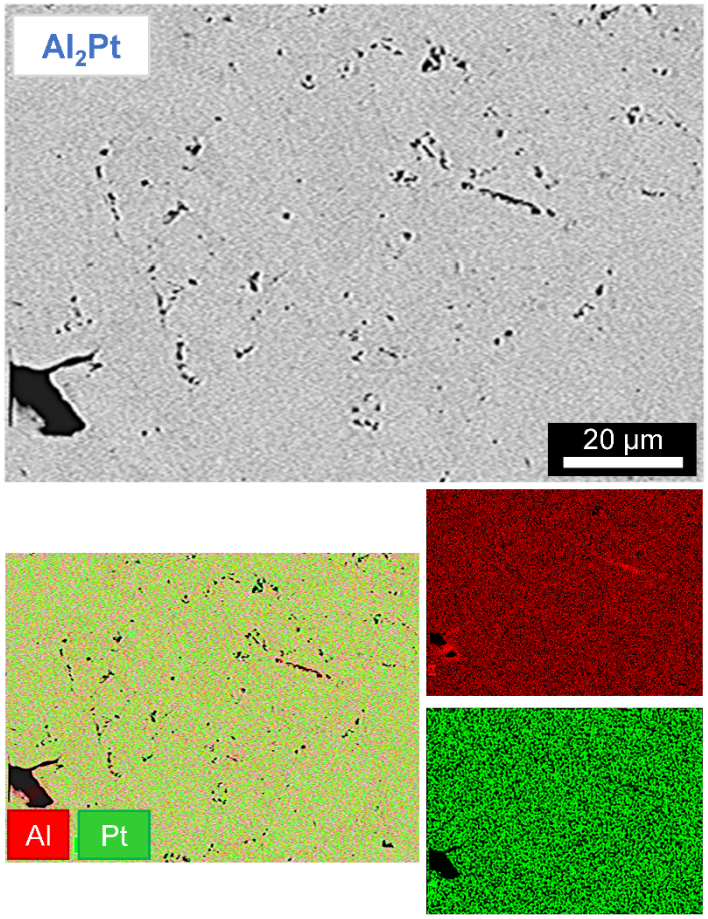
Al_2Pt
20 µm
Al
Pt

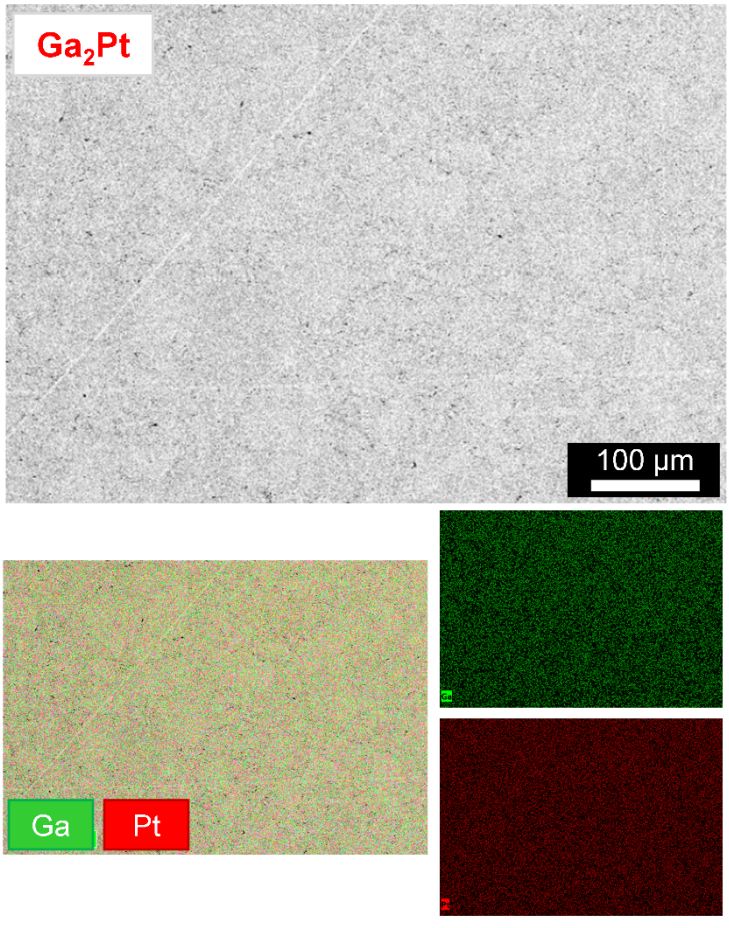
Ga_2Pt
100 µm
Ga
Pt

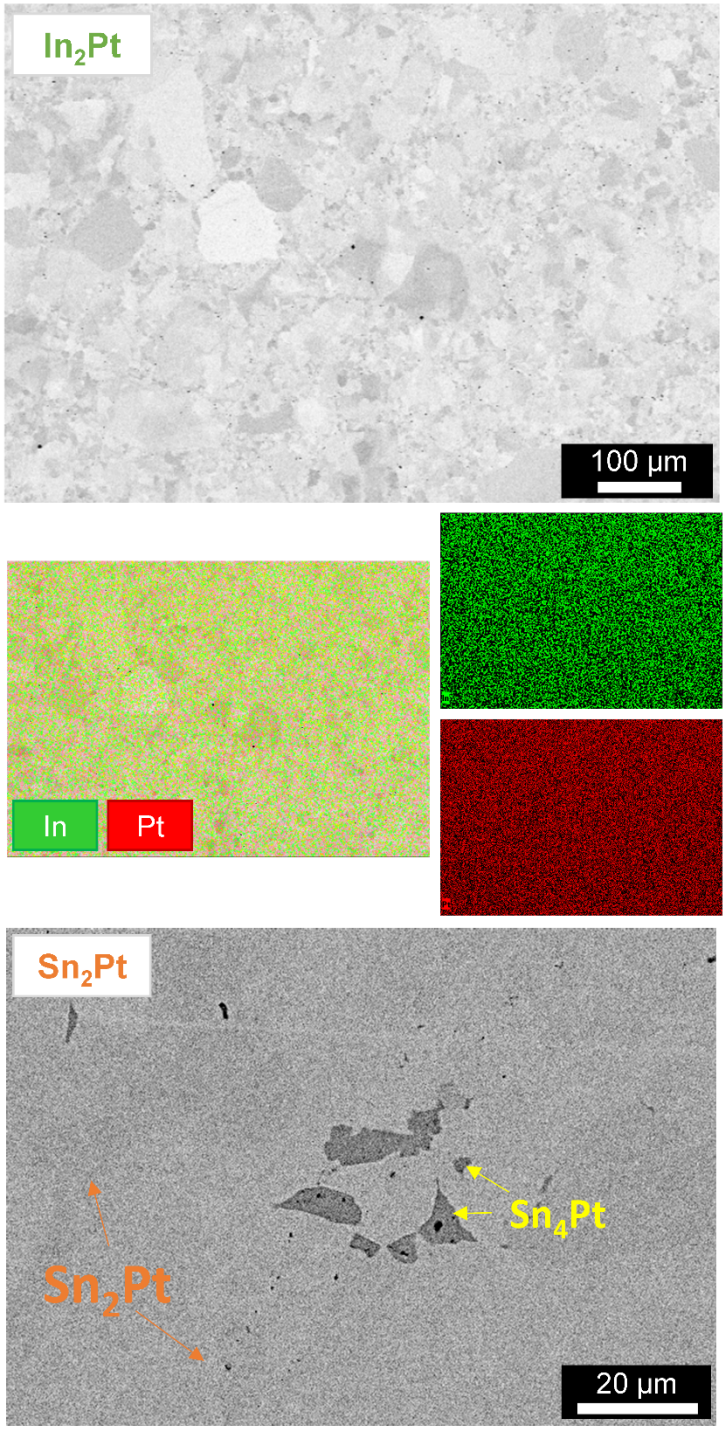

Figure S2. BSE images (material contrast, 27 kV) of the M_2Pt specimens, where *M* is Al (*a*), Ga (*b*), In (*c*) or Sn (*d*), supported by the elemental mapping for Al_2Pt, Ga_2Pt and In_2Pt, revealing the homogeneity of these samples.

The specimen of Sn_2Pt contains negligible amount of secondary Sn_4Pt phase. Its small amount can be concluded from light microscopy image on Figure S1 (tiny bright spots) and absence of corresponding reflections on PXRD pattern (Figure 2).

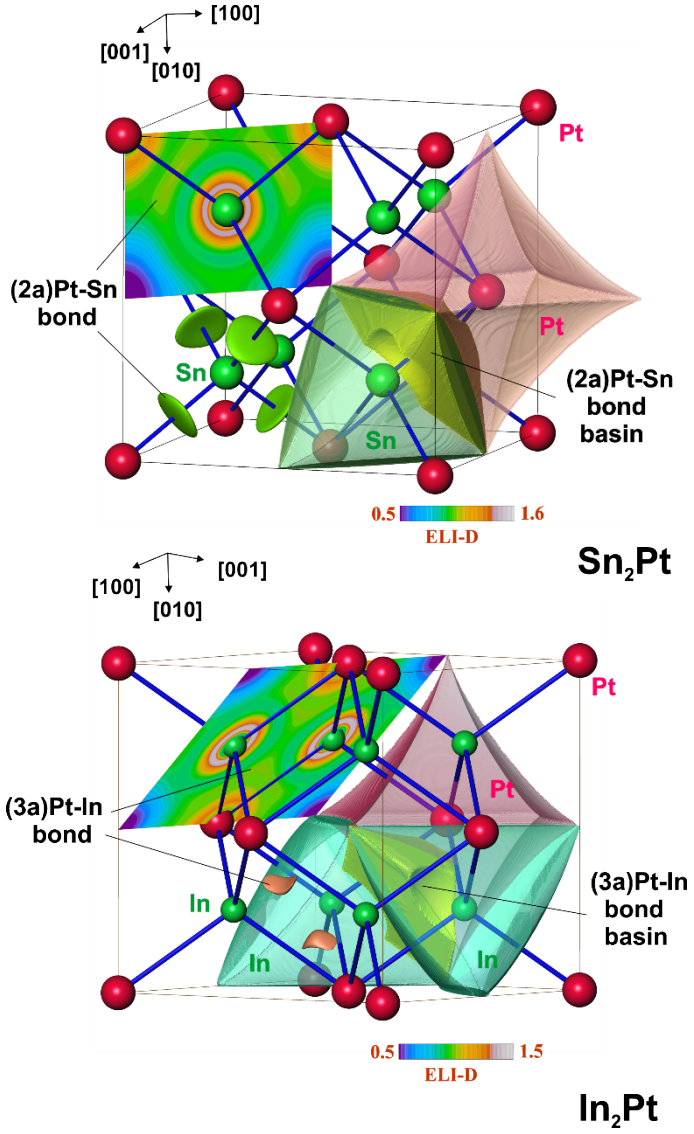

Figure S3. Chemical bonding in Sn_2Pt (*top*) and In_2Pt (*bottom*). Position of the (2a)Pt-Sn and (3a)Pt-In bonds are shown with the ELI-D distributions (*left upper corner*) and isosurfaces (*left bottom corner of each panel*). Bonding basins of these bonds (*yellow*) are shown in overlap with the QTAIM atomic shapes of Pt and Sn for Sn_2Pt (*top*), and Pt and two In for In_2Pt (*bottom*).

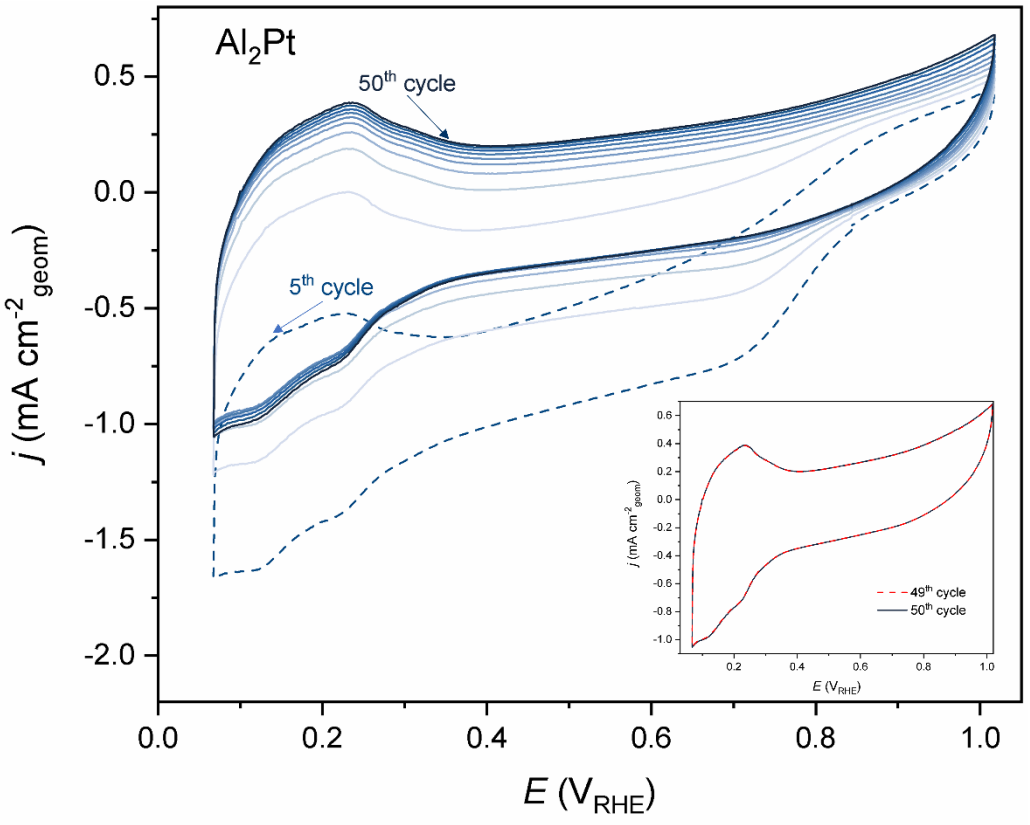
Al2Pt
50th cycle
5th cycle
j (mA cm-2geom)
E (VRHE)
49th cycle
50th cycle

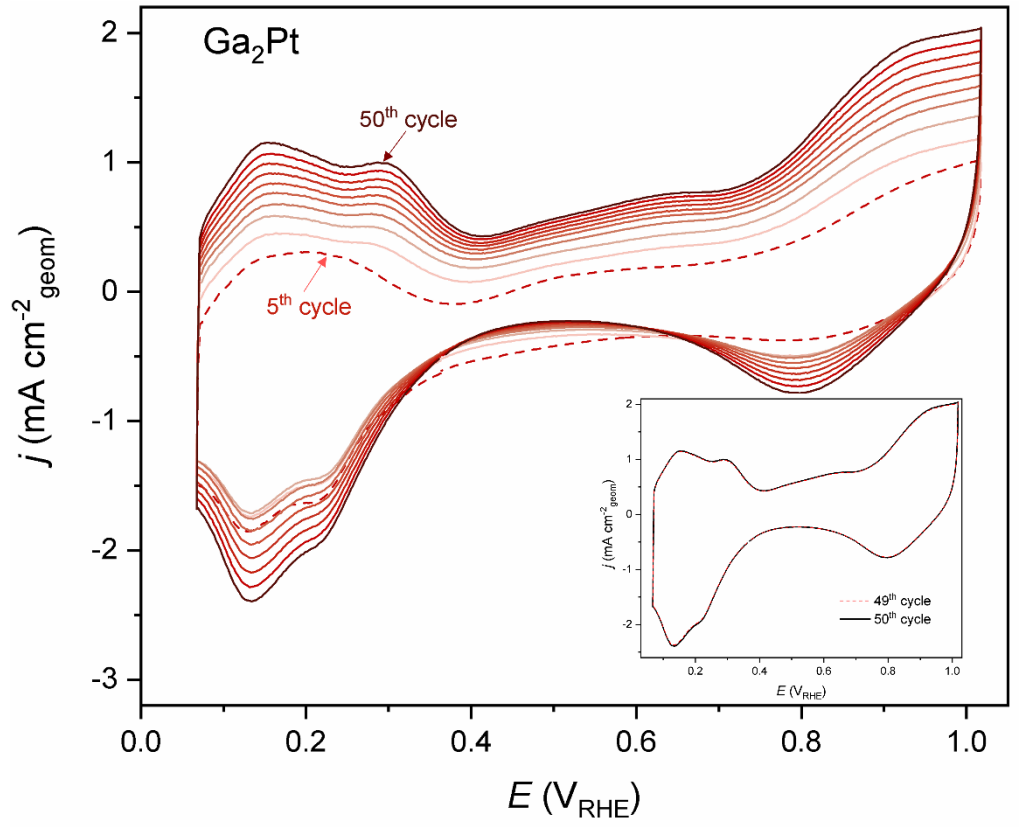
Ga2Pt
50th cycle
5th cycle
j (mA cm-2geom)
E (VRHE)
49th cycle
50th cycle

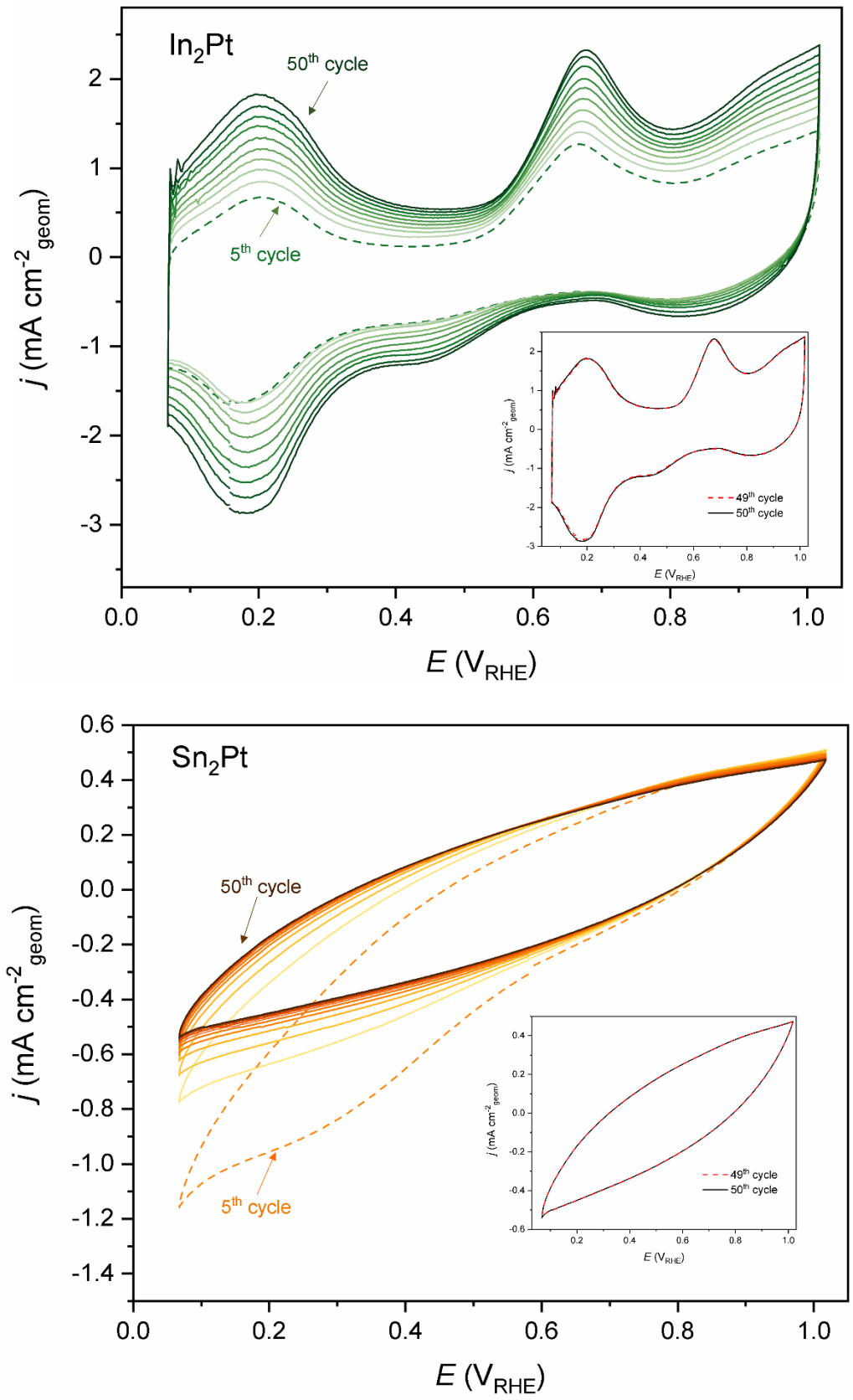

Figure S4. Every 5th CV cycle (0.1 M $HClO_4$; 0.05–1.0 V_{RHE}; 50 mV s^{-1}) for the M_2Pt (M = Al, Ga, In, Sn) compounds. The fifth cycle is presented with *dashed* line and following cycles are presented with the *solid* lines of increasing intensity of corresponding colour. Insets: 49th and 50th CV cycles for M_2Pt.

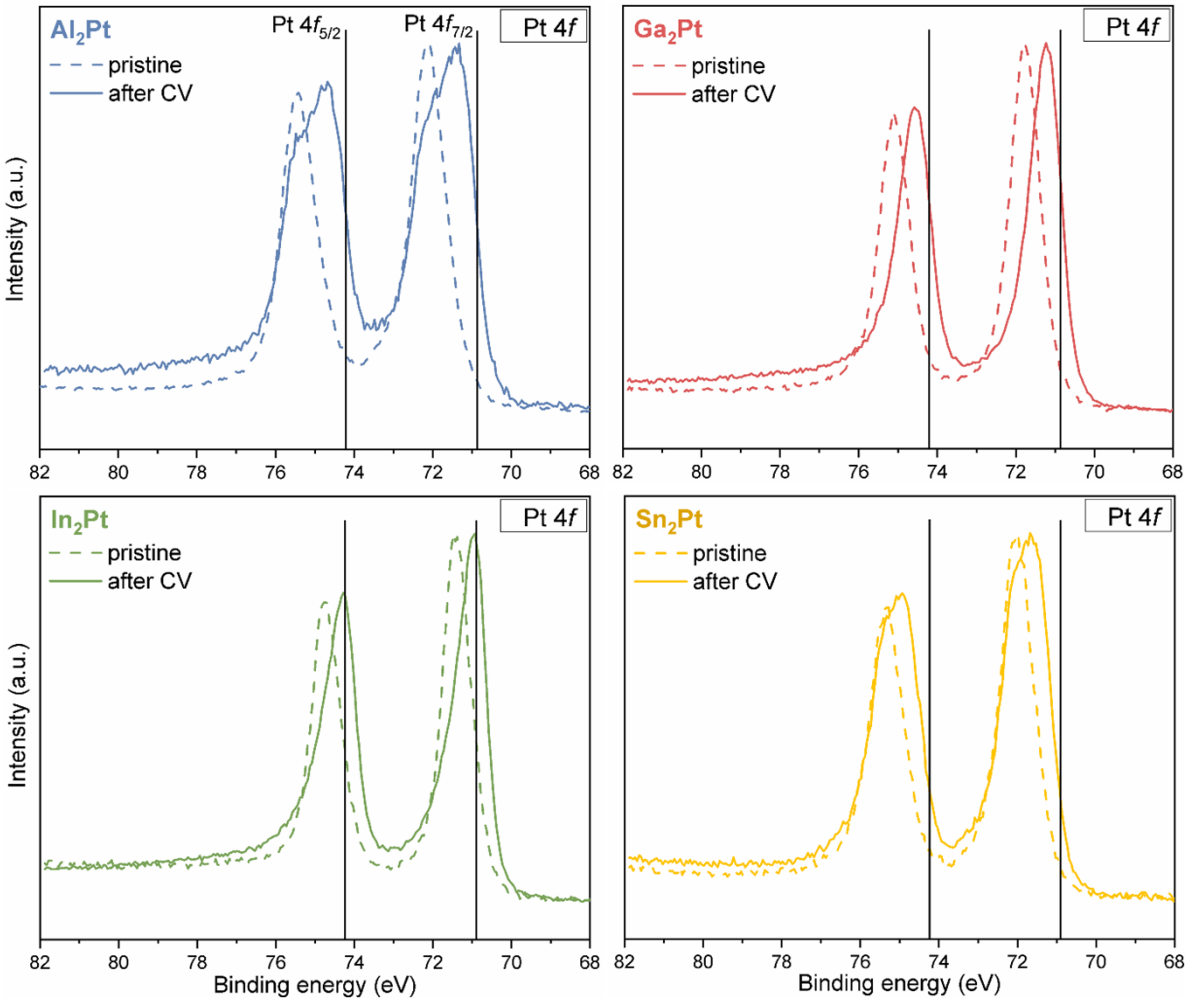

Figure S5. Normalized XPS spectra of Pt 4*f* core levels for the M_2Pt compounds before (*dashed lines*) and after CV (*solid lines*). The vertical solid lines represent the position of Pt 4*f* core levels in elemental Pt.

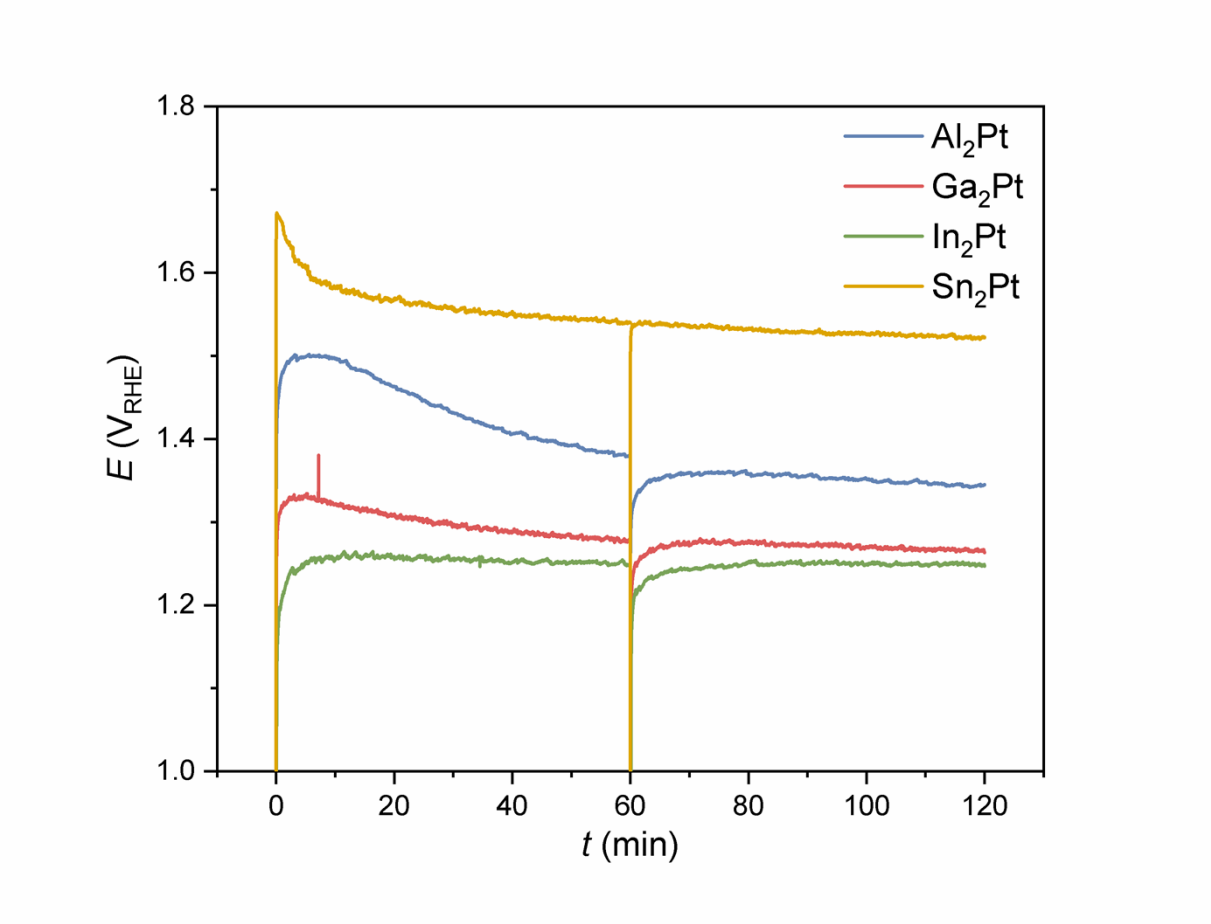

Figure S6. Chronopotentiometry, measured at 10 mA cm^{-2} during 2 h, for the M_2Pt compounds.

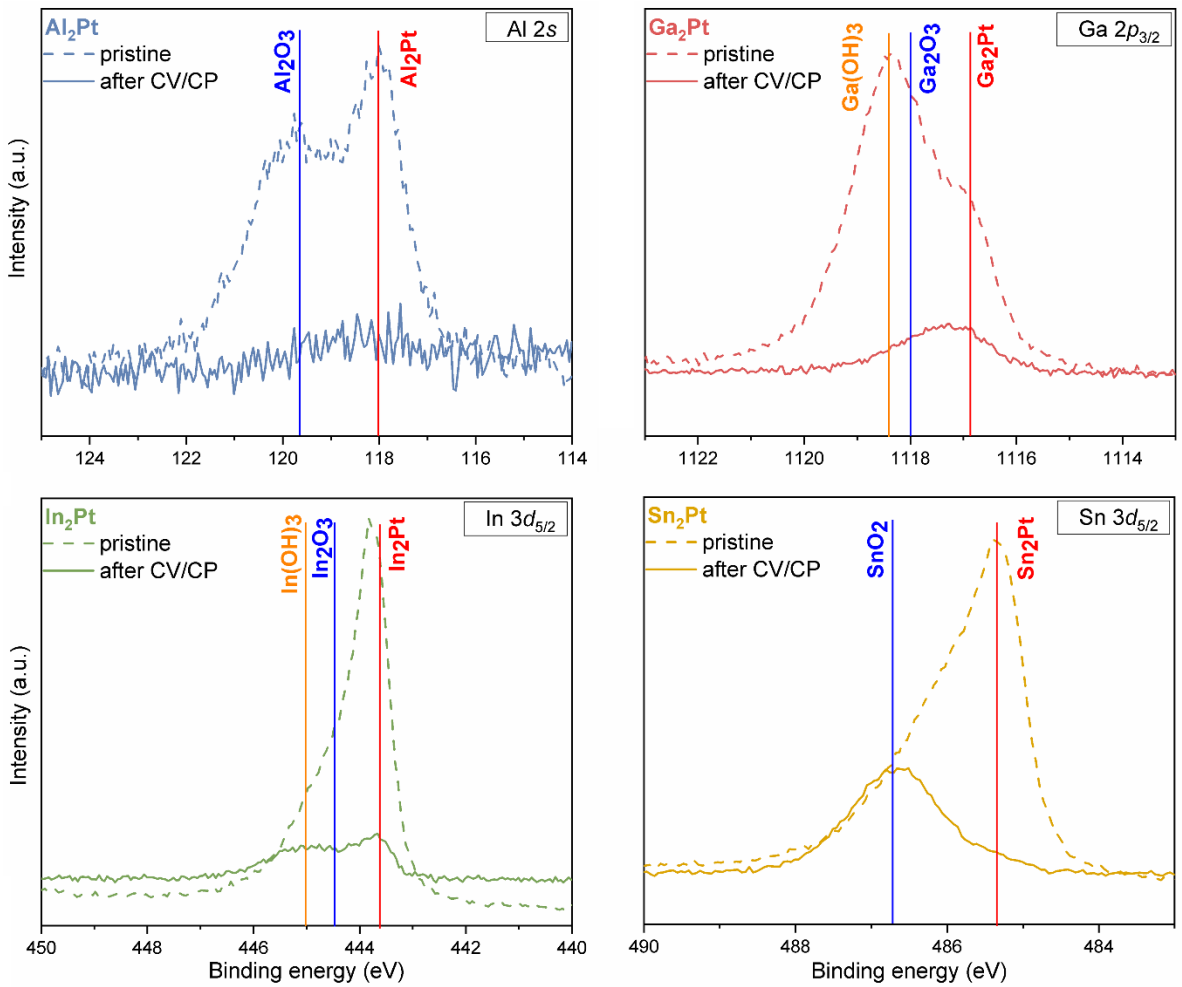

Figure S7. XPS spectra of *M* core levels in M_2Pt compounds before (*dashed lines*) and after the standard OER experiment (*solid lines*). The vertical solid lines represent the binding energies for M_2Pt, M_xO_y oxides and $M(OH)_x$ hydroxides.

The Al spectra after electrochemical experiments are very difficult to interpret because of the overlap of Al 2*p* core level with the intense Pt 4*f* one, and complication of Al 2*s* detection due to the small cross section of this orbital.[1,2] Additionally, its detection is hampered by its significantly reduced amount due to the pronounced dissolution, as observed from elemental analysis of the effluent electrolyte.

$Ga(OH)_3$ signal is significantly reduced on the Ga_2Pt surface after the standard OER experiment. There are two possibilities for that: (i) dissolution in acidic media due to its amphoteric nature,[3,4] and/or (ii) further surface transformation to Ga_2O_3 during the CP measurement.

$In(OH)_3$ is a basic hydroxide, it reacts with acids to give indium salts. However, indates are hydrolyzed back in water to regenerate the hydroxide[4] and, therefore, they are present on the In_2Pt surface.

In case of Sn_2Pt, the surface is covered by SnO_2 layer, which impedes access to the Pt, and, therefore, during the CV measurement the Pt oxidation/reduction features are not observed. SnO_2 is well known as catalyst support for the OER in acidic media due to its outstanding stability.[5] However, it is electrochemically inert and has poor electronic conductivity, and it is commonly doped with other elements to improve its conductivity.[6-8] Therefore, the coverage of Sn_2Pt surface by the poorly conductive SnO_2 hinders the electron transfer and leads to OER inactivity of Sn_2Pt.

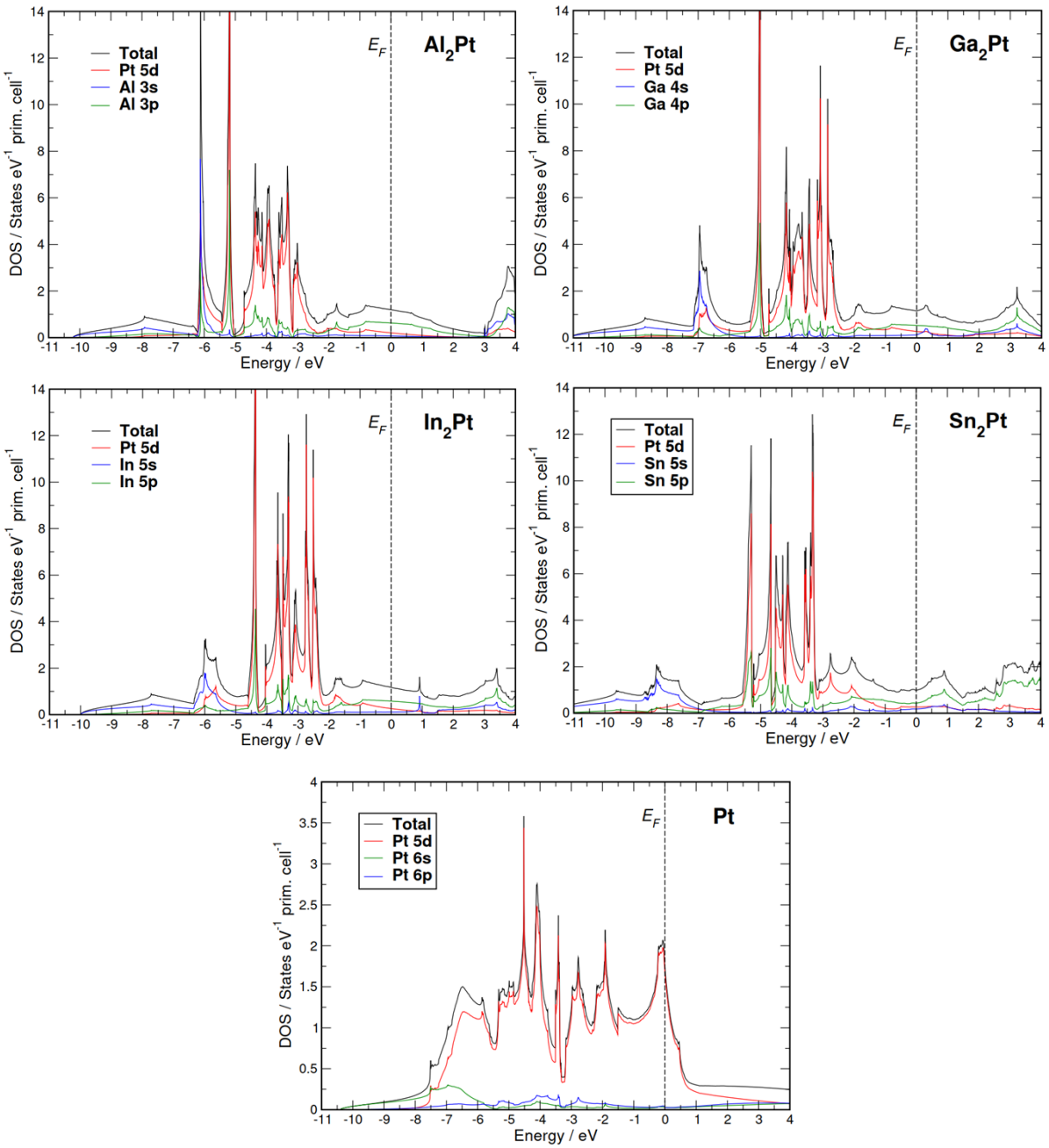

Figure S8. Calculated total and orbital projected DOS for the M_2Pt compounds and *fcc* Pt at the fully-relativistic level.

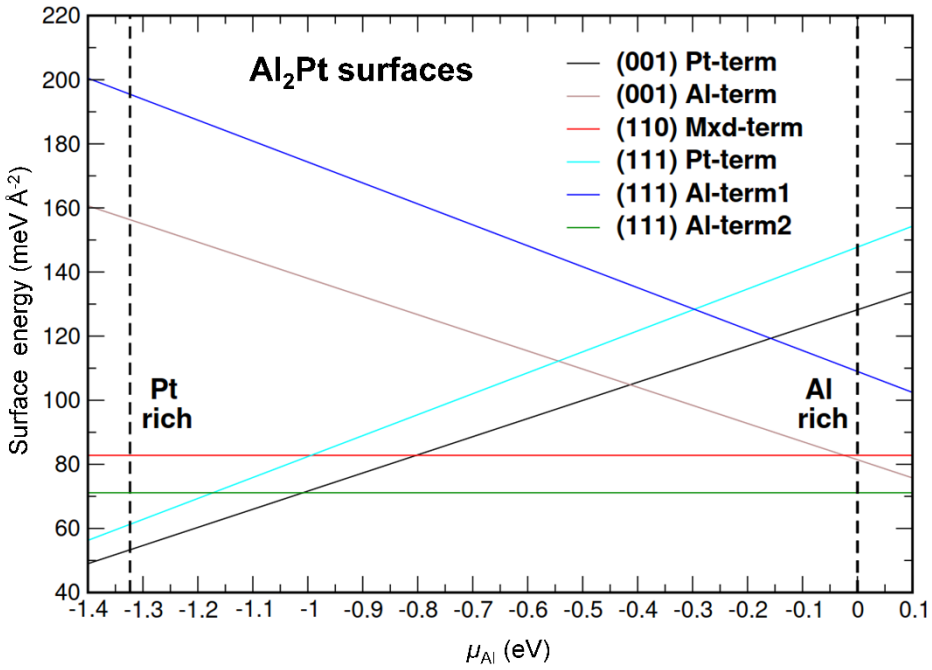

Figure S9. Surface energies of the different Al_2Pt surfaces versus the chemical potential of Al.

Table S1. OER performance of selected bulk OER electrocatalysts in acidic media: overpotential at 10 mA cm^{-2} (otherwise indicated with the subscript of η) as activity marker, and time of the chronopotentiometry (CP) or chronoamperometry (CA) operation at j = 10 mA cm^{-2} (otherwise indicated) as stability marker.

Electrocatalyst	**Electrolyte**	**Activity** η_{10} (mV)	**Stability** t (h)	**Ref.**
Noble metal - (based) OER electrocatalysts				
Ru	0.1 M $HClO_4$	219 ($\eta_{0.5}$)	-	9
	0.1 M H_2SO_4	255 ($\eta_{0.8}$)	1.2 (j = 0.1-1.6 mA cm^{-2})	10
Ir	0.1 M $HClO_4$	321 ($\eta_{0.5}$)	-	9
	0.1 M H_2SO_4	390 ($\eta_{0.8}$)	1.2 (j = 0.1-1.6 mA cm^{-2})	10
*IrO_x / $SrIrO_3$	0.5 M H_2SO_4	270-290	30	11
$Hf_2B_2Ir_5$	0.1 M H_2SO_4	360	240 (j = 100 mA cm^{-2})	12
Rh	0.1 M H_2SO_4	590 ($\eta_{0.8}$)	-	10
Pd	0.1 M H_2SO_4	665 ($\eta_{0.8}$)	-	10
Pt	0.1 M $HClO_4$	536 ($\eta_{0.5}$)	-	9
	0.1 M H_2SO_4	755 ($\eta_{0.8}$)	1.2 (j = 0.1-1.6 mA cm^{-2})	10
Al_2Pt	0.1 M $HClO_4$	623 ø	2	*This work*
	0.1 M $HClO_4$	450 ø	456 (j = 90 mA cm^{-2})	13
Ga_2Pt	0.1 M $HClO_4$	540	2	*This work*
In_2Pt	0.1 M $HClO_4$	520	2	*This work*
Au	0.1 M H_2SO_4	870 ($\eta_{0.8}$)	-	10
**α-AuOOH	0.1 M H_2SO_4	620 ($\eta_{0.1}$)	-	14
Transition metal - based OER electrocatalysts				
*γ-MnO_2	1 M H_2SO_4	480	8000	15
*$Mn_{0.67}Sb_{0.33}O_z$	1 M H_2SO_4	586	2	16
*$MnSb_{1.7}O_y$	1 M H_2SO_4	727	168	17
*Ti-MnO_2	0.05 M H_2SO_4	520 ($\eta_{1.0}$)	265 (E = 1.8 V_{RHE})	18
*$(Ti,Mn)O_x$	1 M H_2SO_4	437 ($\eta_{0.9}$)	210 (E = 1.67 V_{RHE})	19
*$Co_{0.05}Fe_{0.95}O_y$	0.5 M H_2SO_4	660	50	20
*Fe_2O_3	0.5 M H_2SO_4	650	24	21
Fe_2Ta	0.5 M H_2SO_4	770	-	22
Co_2Ta	0.5 M H_2SO_4	600	-	22
Ni_2Ta	0.5 M H_2SO_4	570	65	22
*$Ni_xMn_{1-x}Sb_{1.6-1.8}O_y$	1 M H_2SO_4	670-800	168	17

*Film

**Electrochemically prepared

ø Different pre-treatments

Table S2. The XPS binding energies of Pt $4f_{7/2}$ core levels (BE_{4f}) and their shifts ($\delta(BE_{4f})$, with respect to elemental Pt) in the intermetallic M_2Pt compounds.

Compound	Initial		After CV		After CV+CP	
	BE_{4f}, eV	**$\delta(BE_{4f})$, eV**	**BE_{4f}, eV**	**$\delta(BE_{4f})$, eV**	**BE_{4f}, eV**	**$\delta(BE_{4f})$, eV**
Al_2Pt	72.12	1.12	71.4	0.4	71.14	0.14
Ga_2Pt	71.77	0.77	71.22	0.22	71	0
In_2Pt	71.42	0.42	71	0	71	0
Sn_2Pt	72.02	1.02	71.64	0.64	71.36	0.36

Table S3. Calculated (for homogeneous M_2Pt) and experimentally obtained (with EDXS, for samples after the standard OER experiment) intensities of the *M* line spectra (in cps/eV) normalized to the Pt *M*α (using different acceleration voltages).

Spectral line	5 kV		10 kV		27 kV	
	I calc.	*I* exp.	*I* calc.	*I* exp.	*I* calc.	*I* exp.
Al *K*α	1.44	0.21	1.07	0.35	0.91	0.65
Ga *L*α	2.89	0.32	1.70	0.12	1.36	0.04
In *L*α	0.19	0.02	0.59	0.02	0.91	0.03
Sn *L*α	0.13	0.18	0.54	0.58	0.91	0.99

References:

1. M.B. Trzhaskovskaya, V.I. Nefedov, V.G. Yarzhemsky, *At. Data Nucl. Data Tables*, 2001, **77**, 97-159.
2. M.B. Trzhaskovskaya, V.K. Nikulin, V.I. Nefedov, V.G. Yarzhemsky, *At. Data Nucl. Data Tables*, 2006, **92**, 245-304.
3. S. Aldridge, A.J. Downs, *The Group 13 Metals Aluminium, Gallium, Indium and Thallium: Chemical Patterns and Peculiarities*, John Wiley & Sons, UK, 2011.
4. A.J. Downs, *Chemistry of aluminium, gallium, indium and thallium*, Blackie academic and professional, UK, 1993.
5. S. Geiger, O. Kasia, A.M. Mingers, K.J.J. Mayrhofer, S. Cherevko, *Sci. Rep.*, 2017, **7**, 4595-1-7.
6. G. Liu, J. Xu, Y. Wang, X. Wang, *J. Mater. Chem. A*, 2015, 3, 20791-20800.
7. H. Ohno, S. Nohara, K. Kakinuma, M. Uchida, H. Uchida, *Catalysis*, 2019, **9**, 74-1-12.
8. S. Abbou, R. Chattot, V. Martin, F. Claudel, L. Sola-Hernandez, C. Beauger, L. Dubau, F. Maillard, *ACS Catal.* 2020, **10**, 7283-7294.
9. T. Reier, M. Oezaslan, P. Strasser, *ACS Catal.*, 2012, **2**, 1765-1772.
10. S. Cherevko, A.R. Zeradjanin, A.A. Topalov, N. Kulyk, I. Katsounaros, K.J.J. Mayrhofer, *ChemCatChem*, 2014, **6**, 2219-2223.
11. L.C. Seitz, C.F. Dickens, K. Nishio, Y. Hikita, J. Montoya, A. Doyle, C. Kirk, A. Vojvodic, H.Y. Hwang, J.K. Nørskov, T.F. Jaramillo, *Science*, 2016, **353**, 1011-1014.
12. A.M. Barrios Jiménez, U. Burkhardt, R. Cardoso-Gil, K. Höfer, S.G. Altendorf, R. Schlögl, Y. Grin, I. Antonyshyn, *ACS Appl. Energy Mater.*, 2020, **3**, 11042-11052.
13. I. Antonyshyn, A.M. Barrios Jiménez, O. Sichevych, U. Burkhardt, I. Veremchuk, M. Schmidt, A. Ormeci, I. Spanos, A. Tarasov, D. Teschner, G. Algara-Siller, R. Schlögl, Y. Grin, *Angew. Chem. Int. Ed.*, 2020, **59**, 16770-16776.
14. S. Yang, D.G.H. Hetterscheid, *ACS Catal.*, 2020, **10**, 12582-12589.
15. A. Li, H. Ooka, N. Bonnet, T. Hayashi, Y. Sun, Q. Jiang, C. Li, H. Han, R. Nakamura, *Angew. Chem. Int. Ed.*, 2019, **58**, 5054-5058.
16. L. Zhou, A. Shinde, J.H. Montoya, A. Singh, S. Gul, J. Yano, Y. Ye, E.J. Crumlin, M.H. Richter, J.K. Cooper, H.S. Stein, J.A. Haber, K.A. Persson, J.M. Gregoire, *ACS Catal.*, 2018, **8**, 10938-10948.
17. I.A. Moreno-Hernandez, C.A. MacFarland, C.G. Read, K.M. Papadantonakis, B.S. Brunschwig, N.S. Lewis, *Energy Environ. Sci.*, 2017, **10**, 2103-2108.
18. R. Frydendal, E.A. Paoli, I. Chorkendorff, J. Rossmeisl, I.E.L. Stephens, *Adv. Energy Mater.*, 2015, **5**, 1500991-1-9.
19. G. Siddiqi, Z. Luo, Y. Xie, Z. Pan, Q. Zhu, J.A. Röhr, J.J. Cha, S. Hu, *ACS Appl. Mater. Interfaces*, 2018, **10**, 18805-18815.
20. W.L. Kwong, C.C. Lee, A. Shchukarev, J. Messinger, *Chem. Commun.*, 2019, **55**, 5017-5020.
21. W.L. Kwong, C.C. Lee, A. Shchukarev, E. Björn, J. Messinger, *J. Catal.*, 2018, **365**, 29-35.
22. J.S. Mondschein, K. Kumar, C.F. Holder, K. Seth, H. Kim, R.E. Schaak, *Inorg. Chem*., 2018, **57**, 6010-6015.